Wavelength-selective addressing of visible and near-infrared plasmon resonances for SU8 nanolithography

Anouk de Hoogh, Bob Hommersom, and A. Femius Koenderink*

Center for Nanophotonics, FOM Institute for Atomic and Molecular Physics (AMOLF), Science Park 104, 1098 XG Amsterdam, The Netherlands

*f.koenderink@amolf.nl

Abstract: We imprint plasmonic near field enhancements as nanoscale topography in SU8 photoresist using two-photon absorption from a spectrally filtered broadband supercontinuum light source. Imprinted patterns smaller than 50 nm across are obtained localized at positions of high local field enhancements in gold bow tie antennas, and gold split rings resonant in the visible and near-infrared. Enhanced exposure only occurs at wavelengths and polarizations that exactly match the plasmonic resonances. Hence our work demonstrates that wavelength selective addressing of hot spots for nanolithography using an inexpensive, low peak-power picosecond pulsed source is freely tunable throughout the visible and infrared to match any desired plasmon resonance.

OCIS codes: (310.6628) Subwavelength structures, nanostructures; (160.3918) Metamaterials; (240.6680) Surface plasmons; (180.4243) Near-field microscopy; (220.4241) Nanostructure fabrication.

References and links

1. W. L. Barnes, A. Dereux, and T. W. Ebbesen, "Surface plasmon subwavelength optics," Nature **424**, 824–830 (2003).
2. S. Lal, S. Link, and N. J. Halas, "Nano-optics from sensing to waveguiding," Nat. Photonics **1**, 641–648 (2007).
3. J. A. Schuller, E. S. Barnard, W. Cai, Y. C. Jun, J. S. White, and M. L. Brongersma, "Plasmonics for extreme light concentration and manipulation," Nature Mater. **9**, 193–204 (2010).
4. J. N. Anker, W. P. Hall, O. Lyandres, N. C. Shah, J. Zhao, and R. P. Van Duyne, "Biosensing with plasmonic nanosensors," Nature Mater. **7**, 442–453 (2008).
5. H. A. Atwater and A. Polman, "Plasmonics for improved photovoltaic devices," Nature Mater. **9**, 205–213 (2010).
6. A. Sundaramurthy, P. J. Schuck, N. R. Conley, D. P. Fromm, G. S. Kino, and W. E. Moerner, "Toward nanometer-scale optical photolithography: utilizing the near-field of bow tie optical nanoantennas," Nano Lett. **6**, 355–360 (2006). PMID: 16522022.
7. O. J. F. Martin, "Surface plasmon illumination scheme for contact lithography beyond the diffraction limit," Microelectron. Eng. **67–68**, 24–30 (2003).
8. W. Srituravanich, N. Fang, C. Sun, Q. Luo, and X. Zhang, "Plasmonic nanolithography," Nano Lett. **4**, 1085–1088 (2004).
9. N. Fang, H. Lee, C. Sun, and X. Zhang, "Sub-diffraction-limited optical imaging with a silver superlens," Science **308**, 534–537 (2005).
10. D. B. Shao and S. C. Chen, "Direct patterning of three-dimensional periodic nanostructures by surface-plasmon-assisted nanolithography," Nano Lett. **6**, 2279–2283 (2006).
11. K. Ueno, S. Juodkazis, T. Shibuya, Y. Yokota, V. Mizeikis, K. Sasaki, and H. Misawa, "Nanoparticle plasmon-assisted two-photon polymerization induced by incoherent excitation source," J. Am. Chem. Soc **130**, 6928–6929 (2008).
12. N. Murazawa, K. Ueno, V. Mizeikis, S. Juodkazis, and H. Misawa, "Spatially selective nonlinear photopolymerization induced by the near-field of surface plasmons localized on rectangular gold nanorods," J. Phys. Chem. C **113**, 1147–1149 (2009).

#146475 - $15.00 USD Received 26 Apr 2011; revised 20 May 2011; accepted 20 May 2011; published 26 May 2011

13. K. Ueno, S. Takabatake, Y. Nishijima, V. Mizeikis, Y. Yokota, and H. Misawa, "Nanogap-assisted surface plasmon nanolithography," J. Phys. Chem. Lett. **1**, 657–662 (2010).
14. C. Hubert, A. Rumyantseva, G. Lerondel, J. Grand, S. Kostcheev, L. Billot, A. Vial, R. Bachelot, P. Royer, S.-h. Chang, S. K. Gray, G. P. Wiederrecht, and G. C. Schatz, "Near-field photochemical imaging of noble metal nanostructures," Nano Lett. **5**, 615–619 (2005).
15. C. Deeb, R. Bachelot, J. Plain, A.-L. Baudrion, S. Jradi, A. Bouhelier, O. Soppera, P. K. Jain, L. Huang, C. Ecoffet, L. Balan, and P. Royer, "Quantitative analysis of localized surface plasmons based on molecular probing," ACS Nano **4**, 4579–4586 (2010).
16. A. F. Koenderink, J. V. Hernández, F. Robicheaux, L. D. Noordam, and A. Polman, "Programmable nanolithography with plasmon nanoparticle arrays," Nano Lett. **7**, 745–749 (2007).
17. M. Durach, A. Rusina, M. I. Stockman, and K. Nelson, "Toward full spatiotemporal control on the nanoscale," Nano Lett. **7**, 3145–3149 (2007).
18. B. Gjonaj, J. Aulbach, P. M. Johnson, A. P. Mosk, L. Kuipers, and A. Lagendijk, "Digital plasmonics," Nat. Photonics (in press) arXiv:1011.4244 (2011).
19. P. S. J. Russell, "Photonic crystal fibers," Science **299**, 358–362 (2003).
20. A. Sundaramurthy, K. B. Crozier, G. S. Kino, D. P. Fromm, P. J. Schuck, and W. E. Moerner, "Field enhancement and gap-dependent resonance in a system of two opposing tip-to-tip Au nanotriangles," Phys. Rev. B **72**, 165409 (2005).
21. H. Fischer and O. J. F. Martin, "Engineering the optical response of plasmonic nanoantennas," Opt. Express **16**, 9144–9154 (2008).
22. C. Enkrich, M. Wegener, S. Linden, S. Burger, L. Zschiedrich, F. Schmidt, J. F. Zhou, T. Koschny, and C. M. Soukoulis, "Magnetic metamaterials at telecommunication and visible frequencies," Phys. Rev. Lett. **95**, 203901 (2005).
23. C. Rockstuhl, F. Lederer, C. Etrich, T. Zentgraf, J. Kuhl, and H. Giessen, "On the reinterpretation of resonances in split-ring-resonators at normal incidence," Opt. Express **14**, 8827–8836 (2006).
24. T. Zentgraf, J. Dorfmüller, C. Rockstuhl, C. Etrich, R. Vogelgesang, K. Kern, T. Pertsch, F. Lederer, and H. Giessen, "Amplitude- and phase-resolved optical near fields of split-ring-resonator-based metamaterials," Opt. Lett. **33**, 848–850 (2008).
25. D. Diessel, M. Decker, S. Linden, and M. Wegener, "Near-field optical experiments on low-symmetry split-ring-resonator arrays," Opt. Lett. **35**, 3661–3663 (2010).
26. G. Boudarham, N. Feth, V. Myroshnychenko, S. Linden, J. G. de Abajo, M. Wegener, and M. Kociak, " Spectral imaging of individual split-ring resonators," Phys. Rev. Lett. **105**, 255501 (2010).
27. I. Sersic, M. Frimmer, E. Verhagen, and A. F. Koenderink, "Electric and magnetic dipole coupling in near-infrared split-ring metamaterial arrays," Phys. Rev. Lett. **103**, 213902 (2009).
28. H. Lorenz, M. Despont, N. Fahrni, N. LaBianca, P. Renaud, and P. Vettiger, "Su-8: a low-cost negative resist for mems," J. Micromech. Microeng. **7**, 121–124 (1997).
29. G. Vecchi, V. Giannini, and J. Gómez Rivas, "Shaping the fluorescent emission by lattice resonances in plasmonic crystals of nanoantennas," Phys. Rev. Lett. **102**, 146807 (2009).
30. Y. Bi and D. C. Neckers, "A visible light initiating system for free radical promoted cationic polymerization," Macromolecules **27**, 3683–3693 (1994).
31. P. Banzer,U. Peschel, S. Quabis, and G. Leuchs,"On the experimental investigation of the electric and magnetic response of a single nano-structure," Opt. Express **18**, 10905–10923 (2010).
32. F. Garwe, U. Bauerschäfer, A. Csaki, A. Steinbrück, K. Ritter, A. Bochmann, J. Bergmann, A. Weise, D. Akimov, G. Maubach, J. König, G. Hüttmann, W. Paa, J. Popp, and W. Fritzsche, "Optically controlled thermal management on the nanometer length scale," Nanotechnology **19**, 055207 (2008).
33. K. D. Ko, A. Kumar, K. H. Fung, R. Ambekar, G. L. Liu, N. X. Fang, and K. C. Toussaint, "Nonlinear optical response from arrays of Au bowtie nanoantennas," Nano Lett. **11**, 61–65 (2011).
34. M. W. Klein, M. Wegener, N. Feth, and S. Linden, "Experiments on second- and third-harmonic generation from magnetic metamaterials: erratum," Opt. Express **16**, 8055–8055 (2008).
35. R. de Waele, A. F. Koenderink, and A. Polman, "Tunable nanoscale localization of energy on plasmon particle arrays," Nano Lett. **7**, 2004–2008 (2007).

1. Introduction

Metallic surfaces and scatterers with sub-100 nm features are widely pursued for their very strong response to light [1–3]. Indeed, plasmonic resonances in noble metal nano-scatterers generate very large cross sections for extinction and scattering, and strongly enhanced near fields that are desirable for sensing, surface enhanced Raman scattering, nonlinear effects, single molecule microscopy, as well as for enhancement of photovoltaic efficiencies and light emitting diodes [1–5]. In this field of research, the interaction of plasmon resonances with photore-

#146475 - $15.00 USD Received 26 Apr 2011; revised 20 May 2011; accepted 20 May 2011; published 26 May 2011

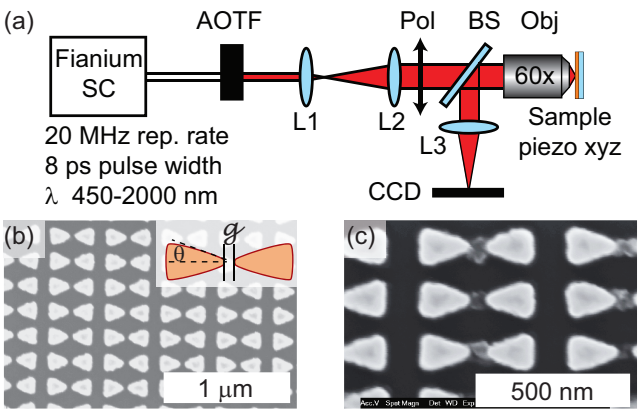

Fig. 1. (a) Our set up consists of a Fianium supercontinuum source (SC), filtered by acousto-optic tunable filters (AOTFs). We expand the beam(telescope lenses L1, L2) and polarize it (Pol), overfill the microscope objective back aperture, and write lines in SU8 by displacing the sample on a piezo stage. A CCD monitors the alignment via beam splitter BS and tube lens L3. (b) Scanning electron micrograph (SEM) of unexposed Au bow ties on sapphire, with gap width g=50 nm and taper half angle θ=20°. (c) Bow ties with polymerized SU8 at the bow tie tips after exposure with 800 nm, 5 mW, polarized along the bow tie, scan speed 0.3 μm/s .

sists is interesting for two reasons. Firstly, a main question in nanophotonics is how to visualize sub-diffraction near-field distributions experimentally, without the perturbative effect of a near field probe. Photoresistive polymers can act as homogeneous dielectric, non-perturbative probes in which a near-field distribution can be written upon single photon, or two-photon absorption. This method was first demonstrated by Sundaramurthy *et al.* [6], who reported the formation of 30 nm voxels in SU8 at the hot spots of bow tie antennas. Similar results have been obtained both with SU8 [7–13], and with azobenzene resists that continuously deform in response to light [14, 15], rather than having a binary response. The second reason for which interaction of plasmons and photoresist is interesting is deep subwavelength optical contact lithography, since plasmonic masks allow sub-50 nm patterning at visible light frequencies [7, 8, 10–13]. Particularly exciting is the prospect of programmable lithography, in which a single mask can give different patterns depending on incident wavelength and polarization [16], or using phasefront shaping [17, 18].

Plasmon-enhanced photolithography naturally requires that the resist, the light source and the plasmon resonance are spectrally matched. Sofar, all approaches with standard photoresists (i.e., SU8) have used either wavelength-integrated lamp exposure [11, 13], or femtosecond pulsed lasers [6, 12]. In the first case even wavelength-integrated power densities are so low that long exposures are required (order 1hr [11]), so no wavelength selection can possibly be applied. Exposure is fast for raster scanning confocal femtosecond illumination schemes as in Ref. [6, 12], but then the wavelength is not widely tunable. While the 800 nm band of Ti:sapphire lasers happens to be matched to, e.g., bow ties, it is highly desirable to achieve polymerization using an inexpensive, ultra-bright and spectrally tunable illumination that can be matched to any plasmon resonance. In this work we demonstrate that supercontinuum white light sources [19] are excellently suited. After spectral filtering, we can generate plasmon-enhanced resist polymerization in voxels down to 50 nm in size, at any wavelength below 1100 nm using moderate illumination times, provided the illumination exactly matches the res-

#146475 - $15.00 USD Received 26 Apr 2011; revised 20 May 2011; accepted 20 May 2011; published 26 May 2011

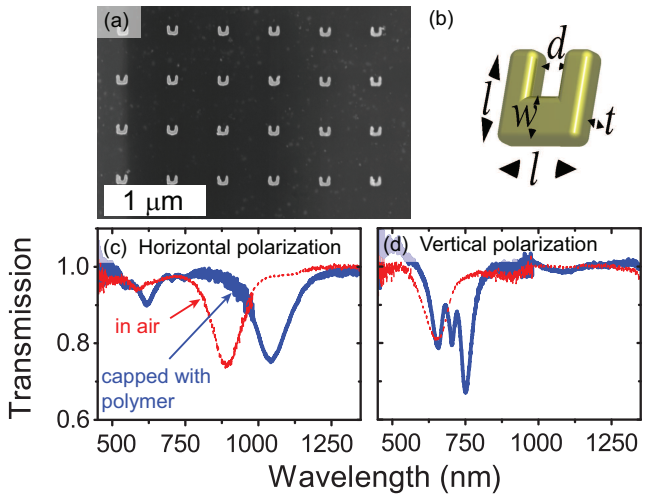

Fig. 2. Scanning electron micrograph (a) and sketch (b) of Au split rings on glass, with dimensions l=100 nm, thickness t =35 nm, gap width d=40 nm and base width w=60 nm. Panels (c,d): Transmission spectra for horizontal and vertical polarization (directions referenced to panel (b)) redshift when embedding the split rings in polymer (blue thick curves) as compared to those for split rings in air on glass (red thin dashed curves). The feature at 1050 nm in (c) is the LC resonance. The splitting at 700 nm is a grating diffraction that is not relevant for focused raster scanning lithography.

onances of our bow ties [6, 20, 21] and split ring resonators (SRRs) [22–27]. This opens the possibility of wavelength-selection based programmable nanolithography.

2. Materials and methods

2.1. Electron beam lithography

We have used electron-beam lithography and a lift-off process after physical vapor deposition of gold in order to define bow ties as well as split rings on sapphire, respectively fused silica substrates. Bare substrates (size 1×1 cm^2) were first cleaned by ultrasonication in water, and immersion in base piranha (H_2O, 30% NH_4OH, 30% H_2O_2, in 5:1:1 ratio) at 75°C for 30 minutes. For e-beam lithography, we spin HMDS primer, a layer of ZEP-520a resist, and finally Espacer 300Z (polythiophene) that acts as conductive layer. The ZEP-520a is diluted 5:2 in anisole and spun for 45 s at 3000 rpm to obtain a resist thickness of 120 nm. Substrates are baked at 180°C for 5 minutes after deposition of ZEP-520a. We perform e-beam exposure in a RAITH e-line electron beam lithography tool by exposing dots positioned on three edges of an 80 nm square, spaced by 10 nm and with 250 aC dose per dot (comparable to a line dose of 250 pC/cm typical for ZEP-520a). After exposure we develop the resist in N-amyl acetate for 1 minute, and subsequently rinse the sample in methylisobutylketone and isopropanol. After physical vapor deposition of gold (pressure 10^{-6} mbar, deposition rate 0.05 nm/s), we perform lift off by immersing the sample in N-methyl-2-pyrrolidone at 65°C for approximately 3 hours.

2.2. SU8 preparation and development

For photolithography experiments, substrates were covered with 300 nm thick layers of SU8 by spincoating (Microchem, 8 wt% in γ-butyrolactone) at 3000 rpm for 45 s, followed by two pre-exposure bake steps at 60°C and 95°C for 60 s each. Samples were mounted in a sample

#146475 - $15.00 USD Received 26 Apr 2011; revised 20 May 2011; accepted 20 May 2011; published 26 May 2011

scanning confocal microscope (SU8 side facing the objective). SU8 polymerization occurs due to photo-acid generation upon photon absorption, whereafter the acid catalyzes polymerization. Final cross-linking is promoted by a post-exposure bake [28] (65°C and 95°C for 60 s each). After baking, the SU8 was developed in MicroChem SU8 developer for 60 s, and inspected in SEM (scanning electron microscope).

2.3. Raster scanning confocal microscope

The home-built confocal microscope (Figure 1(a)) in which exposure was performed consists of a calibrated piezo-electric scanner (Piezojena Tritor 38) that holds the sample, an infinity corrected Nikon objective (CFI S Plan Fluor ELWD 60x/0.7), and a spectrally filtered supercontinuum source. The supercontinuum source (Fianium SC-450PP) provides τ=8 ps pulses at a f=20 MHz repetition rate, and a cw output power of 2 Watt over a spectrum ranging from 450 to 2000 nm. We use acousto-optic tunable filters (polychromatic TeO_2 AOTFs, Crystal Technology) driven with an 8-channel digital RF synthesizer (AODS20160, Crystal Technology) to create a band-pass filter of frequency width $\Delta\omega = 750$ cm^{-1} (30 to 50 nm spectral bandwidth), centered at any desired wavelength from 450 to 1200 nm. The incident beam (powers up to 6 mW) is focused to an almost diffraction limited spot (quality limited by imperfect correction of the objective for the absence of a cover slip). We write isolated lines at scan speeds set between v=0.15 and 4.6 μm/s that start 2 to 3 μm outside the e-beam write fields for reference purposes.

3. Results

3.1. Benchmark: bow tie antennas

Motivated by Ref. [6], we first studied gold bow ties as a benchmark structure. The bow ties are fabricated by e-beam lithography in dense arrays of 450×200 nm pitch, with a bow tie gap of 50 nm, a taper half-angle of 20 degrees, and a gold thickness of 30 nm (Figure 1). Such bow ties have a resonance at 800 nm when illuminated with polarization along the bow-tie axis. A large field enhancement is attained in the gap, with enhancements of $|E|^2$ in the gap ranging from 10^2 to 10^4 times, increasing strongly with narrowing gap width as calculated by several workers using full-wave simulations [6, 20, 21]. Figure 1(c) shows a SEM image of bow tie antennas after exposure at λ=800 nm, with a cw power of 5 mW and a scan speed of 0.3 μm/s. Voxels of SU8 remain after development, with a sub-diffraction limited size of ∼50 nm. These voxels appear solely when the incident polarization for the exposure beam is along the bow tie axis, matching the polarized nature of the resonance, and appear for a broad range of powers, from below 1 to above 5 mW. Such voxels at bow tie hot spots replicate those obtained with a femtosecond Ti:Sapph laser by Sundaramurthy [6]. A significant extension is that they are obtained with a broadband tunable light source at similarly fast exposure rates despite the much lower peak power associated with picosecond sources. SU8 has a single photon absorption edge at 365 nm, so any polymerization is due to multi-photon absorption. SU8 polymerization occurs in two steps. Firstly, multi-photon absorption induces photo-acid generation localized in the region of high intensity. Next, the acid catalyzes polymerization, which is further promoted by a post-exposure bake [28]. We now proceed to estimate the scaling of critical exposure parameters in a line scan geometry. Assuming a total energy W in each laser pulse (taken Gaussian in temporal and spatial profile), the instantaneous irradiance due to pulse N at time t in the xy sample plane when writing a line along x is given by $I_N(x,y,t) = I_0 \exp\left[-\frac{(t-t_N)^2}{2\tau^2}\right] \exp\left[-\frac{(x-vt)^2+y^2}{2w^2}\right]$ where $I_0 = W/[(2\pi)^{3/2} w^2 \tau]$. Also, we define $t_N = N/f$ as the arrival time of pulse N, and w as the beam width. We assume that the probability for a two-photon induced photo-acid generation event occurring in pulse N is $p_N \propto \int dt I_N^2(x,y,t)$, and that the probability for photo-acid generation due to a full pulse sequence is proportional to $\sum_{N=-\infty}^{\infty} p_N$. In the limit that the sample

#146475 - $15.00 USD Received 26 Apr 2011; revised 20 May 2011; accepted 20 May 2011; published 26 May 2011

displacement is small in between subsequent pulses, the probability for a polymerization event at distance y from the line center simplifies to

$$p = \alpha_{\mathrm{SU8}}(\lambda)\frac{W^2}{w^3 v\tau} f \exp(-y^2/w^2), \tag{1}$$

where $\alpha_{\mathrm{SU8}}(\lambda)$ is a wavelength and material-dependent two-photon absorption coefficient. This expression firstly shows that raster scanning reduces exposure times compared to projecting a full line onto the sample (which would replace w^3L by w^2L^2). Secondly, the pulse duration enters linearly in the exposure. This calculation confirms that similar exposures can be obtained with a supercontinuum as with femtosecond (τ=10 ps versus 0.1 ps) lasers, provided the pulse energy W is raised to exceed 5 pJ (above 0.1 mW cw power).

3.2. Split ring resonances from 500 to 1100 nm

Having demonstrated in Figure 1(c) that deep subwavelength ($< \lambda/15$) near-field lithography is possible with a spectrally filtered supercontinuum source despite its low peak power, we now demonstrate the main advantage of such a source. Apart from cost, the main advantage of a supercontinuum source is that it can be tuned to spectrally match any resonance. To explore the large bandwidth over which plasmon-enhanced multi-photon polymerization of SU8 may succeed, we apply raster scanning exposure to gold split rings. In this work we simply use split ring as plasmonic resonators that have a set of distinct localized resonances spread over a wide frequency range [22, 23, 27]. The exact near-field distribution of the field for the different resonances, and in particular the resonances with magnetic character, are of large current interest. This interest is evident from numerical studies [23], as well as experimental efforts to map near fields using near field scanning optical microscopy [24, 25] and electron energy loss spectroscopy in a scanning tunneling electron microscope [26]. We use split rings that are arranged in dilute square arrays of 500×500 nm pitch and 1×1 μm pitch to avoid inter-split ring coupling (Fig. 2(a)). The split rings have a l=100 nm×100 nm size with gold thickness t=35 nm, and gap width d and depth $l-w$ of 40 nm. Figures 2(c,d) show transmission spectra for such arrays of split rings (500 nm pitch). The split rings have a fundamental resonance at approximately 850 nm, when deposited on glass. This fundamental resonance is the LC-resonance of interest to the metamaterials community [22–27], and is only excited with polarization along the base of the SRR. Higher order resonances occur around 500-600 nm, and are plasmonic resonances of the base (Fig. 2(c), λ= 570 nm) and split ring arms (Fig. 2(d), λ= 630 nm) [22]. All resonances redshift upon capping with SU8 as verified from transmission spectra of split ring arrays with and without capping. For such transmission measurements we use the polymer ma-N2400 rather than SU8 as embedding, since exposure of the SU8 (which can not be stripped off after photopolymerization) already during transmission measurements would render the sample useless for subsequent exposure runs. Ma-N2400 has a similar refractive index (n=1.67), but can be stripped off using acetone without any residue or damage. As Figure 2c shows, the fundamental resonance shifts from 850 to 1060 nm. Also the higher order resonances redshift. A rather striking feature is that the higher order resonance at 700 nm splits upon overcoating with polymer. We note that this is a grating diffraction anomaly that occurs when the incident beam couples into the lowest grating diffraction orders that become grazing in the glass substrate at $\lambda = 750$ nm. This diffractive effect is prominent only for vertical polarization, i.e., when the grating resonance overlaps with a single building block resonance [29]. The diffractive effect plays no role in photolithography measurements (below), since it is an artefact of transmission measurements specific for the use of plane wave incident illumination. For photolithography the incident beam is focused on just a single split ring (spot size far below the grating unit cell).

#146475 - $15.00 USD Received 26 Apr 2011; revised 20 May 2011; accepted 20 May 2011; published 26 May 2011

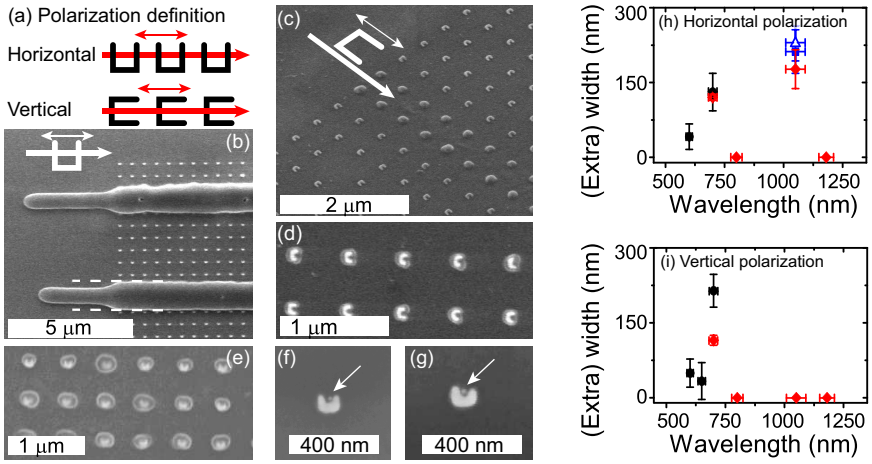

Fig. 3. (a) We scan from left to right with polarization along the scan direction. In this paper 'horizontal (vertical) polarization' means: split ring base along (normal to) the polarization vector. (b) SEM micrograph of split rings (oriented as in Fig. 2(a), top panel) exposed well above the critical dose for SU8 on bare glass (λ=700 nm, power 3.1 mW, v=1.15 and 0.46 μm/s for upper and lower line, horizontal polarization). The lower line broadens from 600 nm to 1 μm. Similar line broadening was observed for 600, 650 and 700 nm. (c) SEM micrograph (angled view) of split rings exposed just below the critical dose for bare glass (λ=700 nm, 1 mW, vertical polarization). Isolated voxels fully enclosing split rings are observed. (d) Top view of voxels observed under conditions as in (c). (e) For λ=1050 nm (on the LC resonance) exposure also induces voxels around split rings, (power 5 mW, scan speed 0.46 μm/s, horizontal polarization). Panels (f, g): When exposed well below the critical dose (0.5 mW), resonance enhancement generates SU8 voxels between the SRR arms when excited at the LC resonance λ=1050 nm. (h,i) Feature size versus wavelength for polarization along the SRR base (h) and along the arms (i). Black squares: line broadening Δy at incident power just above the critical dose Red diamonds: voxel diameter for exposure just below the bare-glass critical dose. Results do not depend strongly on scan speed (0.46 μm/s for all data except square and triangle at 1050 nm (0.2 and 0.33 μm/s)). Horizontal error bars: AOTF bandwidth.

3.3. Resonance selective exposure

We have performed photolithography experiments on SRRs at different wavelengths from 550 to 1100 nm, at power densities just above, just below, and well below the critical dose for SU8 on bare glass. For wavelengths above 800 nm, only data at power densities just below and well below the critical dose on bare glass are reported, as our supercontinuum laser source did not provide sufficient power (below 6 mW) to exceed the critical dose for SU8 on bare glass at those wavelengths. In the case (Fig. 3(b)) of exposure above the bare glass critical dose, lines are already written on the glass next to the SRR arrays, the width of which provides a reference for the exposure enhancement. At specific wavelengths, such as λ=700 nm resonant with the higher order SRR modes, these lines broaden considerably upon entering the split ring arrays, indicating a significant average field enhancement throughout the array. In the second case, i.e., with power density just below the critical dose for SU8 on bare glass, no lines appear outside the split ring arrays. Instead, for specific wavelengths (notably λ=700 nm (Figure 3(c,d)) and 1060 nm (Fig. 3(e)) for polarization along the SRR base) a band appears on the SRR arrays in which each individual split ring is enclosed in an SU8 voxel of approximately 150 to 250 nm total diameter. This observation shows that the field enhancement is localized at the split rings, as

#146475 - $15.00 USD Received 26 Apr 2011; revised 20 May 2011; accepted 20 May 2011; published 26 May 2011

expected. We attempt to derive a quantitative measure for photonic enhancement independent of resist properties from the logarithm of Eq. (1) through $y_{\text{field}}^2 - y_{\text{glass}}^2 = w^2 2\ln(W_{\text{field}}/W_{\text{glass}})$. For small line broadening $\Delta y = y_{\text{field}} - y_{\text{glass}}$, this expression linearizes to $\Delta y \approx 2w\ln(W_{\text{field}}/W_{\text{glass}})$, a relation which is indeed supported by exposure runs on bare glass at different exposure powers W and writing speeds (results not shown). On this basis, we plot the difference Δy in line width for different exposure wavelengths and for two polarizations in Figures 3(h,i), at incident power fixed just above the critical dose. Line broadenings of 200 nm are consistent with a field intensity ($|E|^2$) enhancement of $\sim$30%. It should be noted that this is a lower bound on the enhancement throughout the entire unit cell of the SRR lattice, and is not a measure for the maximum local field enhancement, which is expected to be much higher and which is attained in the split ring gap for $\lambda \sim 1050$ nm (see below). It should be noted that the SU8 itself limits the dynamic range of field enhancements that can be *quantitatively* measured, since only runs that have a power density above the critical dose on bare glass directly provide a reference value y_{glass}. From those runs that had a power density below the critical dose on bare glass, no reference value y_{glass} is available. Instead we take Δy equal to the voxel diameter. Figure 3(h,i) shows that a photonic enhancement of SU8 exposure, i.e. $\Delta y > 0$, is only observed in those cases in which both incident wavelength and polarization match a resonance that is also evident in transmission. While the lack of reference means we can not assess the field enhancement directly, we note that a comparison of incident powers suggests a local enhancement of $|E|^2$ of at least a factor three throughout the entire polymerized domain around the split ring in Fig. 3(c-e). The correlation between polymerization and resonance wavelength shows that nanoscale photolithography is indeed enhanced by plasmonic resonances that can be addressed selectively on the basis of polarization and wavelength over a very wide range, including the full UV/VIS to near infrared. Further improvement of this range may be obtained by mixing the SU8 with red-absorbing photo-acid generating dyes [30].

3.4. Smallest achievable features and programmable lithography

Our result that different resonances in the same system can be addressed by wavelength selection opens the road to programmable lithography on sub-100 nm length scales. In such a scheme, a single mask could give rise to different exposed patterns, simply by addressing different collective resonances, and superpositions thereof, by tuning incident wavelength, polarization and angle. Our conclusion that using standard SU8, a huge bandwidth from 500 to 1100 nm can be addressed, allows significant freedom in designing progammable lithography masks. We note that for the resonators and exposure doses used in this work, the exposed patterns at different resonance wavelengths are not highly distinct from each other, as the exposed patterns consist of fully enclosed split rings (compare Fig. 3(d) and (e)), enclosed in SU8 voxels of circa 200 nm diameter. These voxels are much smaller than the diffraction limited signature of each split ring evident in reflection confocal imaging [31] of the same structures (spot size λ/2NA$\sim$500 to 750 nm depending on wavelength, data not shown), evidencing the role of near field enhancement in the imprinting mechanism. It is not immediately evident why the imprinted field patterns do not appear to show a photonic characteristic that is clearly distinct between resonances. We offer two possible explanations. Firstly, indistinct patterns are expected if polymerization works through some other effect than two photon absorption. For instance, one might expect photothermal broadening effects in which enhanced absorption at photonic resonances would cause a large temperature rise, and thereby polymerization. Thermal effects are distinguished from photonic effects by the fact that any SU8 temperature rise is expected to be confined to a < 20 nm shell everywhere around the metal structure, as opposed to being confined to the optical hot spots [32]. Our observations hence show that thermal effects are certainly negligible for the bow ties, but may play a role for SRRs. We expect absorbed powers

#146475 - $15.00 USD Received 26 Apr 2011; revised 20 May 2011; accepted 20 May 2011; published 26 May 2011

per SRR up to 0.5 pJ per pulse, which could raise the temperature of the gold by $\sim 10^2$ K. This rise is insufficient to, e.g., deform the gold. Due to rapid thermalization in substrate and resist, any thermal effect only lasts for a very short cumulative time (beam dwell time $\times$ duty cycle < 0.1 s) making thermal broadening effects in SU8 due to direct curing or enhanced photo-acid diffusion unlikely. An alternative mechanism that could be suspected apart from two photon absorption in SU8 would be direct absorption of high energy photons that could be created at the metal structures due to non-linear processes. Indeed, several workers reported enhanced second harmonic generation (SHG) at bow ties and split rings [33, 34]. We calculate from the Microchem SU8 datasheet that SU8 requires about 10^5 cross links to be generated in a $50\times50\times50$ nm^3 volume for such a volume to remain after exposure. The optical absorption coefficient of SU8, even at its peak in the UV, implies that only less than 10^4 photons that are injected will actually be absorbed to give rise to cross linking, implying that a total SHG production of at least 10^9 photons per bow tie or SRR would be required. We provide an input flux of 10^{16} fundamental photons per bow tie or split ring. Reported SHG yields for plasmonic and split ring structures [33, 34] are not higher than 10^{-11}. Also after correcting reported yields for the difference in pulse energy, spot size and pulse duration, we find that photo-absorption after SHG generation is likely several orders of magnitude weaker than direct two-photon absorption in SU8. Having excluded exposure mechanisms other than two-photon absorption, the fact remains that exposed patterns at different resonance wavelengths are not highly distinct from each other, as in all cases split rings are fully enclosed in SU8. As an alternative explanation for the full enclosure of split rings in SU8, it may be simply due to the fact that the level sets of constant electromagnetic energy density that we probed are not highly distinct for the different resonances. In that case one expects that lowering of the power would allow to zoom in on more localized features, such as field enhancement expected in the split ring gap at $\lambda = 1060$ nm. In several runs where we tuned the incident power with a ramp during line scanning over the sample, we indeed found a handful of split rings in which voxels truly confined to the split ring gap (size between 20 and 40 nm, smaller than $\lambda/25$, see Figures 3(f,g)) were exposed. These localized voxels occur at incident powers that are tenfold below the incident powers required to fully enclose split rings, suggesting that they correspond to enhancements of $|E|^2$ that are at least tenfold. In part, the rarity of the observations of these localized voxels may be due to the fact that such voxels, if generated, are difficult to locate in electron microscopy, and the fact that such tall and narrow features show poor adhesion to the substrate. In part, we also believe that such voxels are rare due to the narrow dose range in which they occur. This problem is exacerbated by inherent variations in geometry, and hence varying field enhancement from split ring to split ring. The presence of such disorder is also apparent as variations in voxel size in Figure 3(e). We hence propose that nanoscale photolithography can be a sensitive tool to quantify disorder-induced resonance variations in sets of nominally identical resonant nano-structures.

4. Conclusions

To conclude, we reported wavelength- and polarization selective plasmon-enhanced photolithography that allows resonances from 500 to 1100 nm wavelength to be imprinted in SU8. Viewed as a characterization tool for nanophotonics, this method allows to image the near field profile of plasmonic and metamaterial resonators over a very large frequency bandwidth. While photolithographic imprinting of near fields readily provides lower bounds on field enhancement and the volume throughout which enhancement occurs, it is a major challenge to obtain reproducible field enhancement factors in strongly localized hot spots. Photolithographic imprinting may be a useful technique to quantify field strength variations in fabricated structures that occur due to ubiquitous fabrication disorder in nanoscale plasmonic and metamaterial resonators. Viewed in the context of nanolithography, our result promises significant

#146475 - $15.00 USD Received 26 Apr 2011; revised 20 May 2011; accepted 20 May 2011; published 26 May 2011

improvements of the sub-diffraction patterning of SU8 offered by plasmonic contact lithography as proposed in [6, 7, 10, 11, 13]. While the absolute feature size that has been demonstrated with this method remains slightly larger than feature sizes that can be obtained with state of the art electron beam lithography (down to 10 nm), it is remarkable that the achievable feature size can be as small as < 40 nm, i.e., $< \lambda/25$, even at 1100 nm wavelength. This achievement paves the way to fabricating truly nanoscale structures by plasmonic contact lithography using cheap light sources, such as modelocked fiber lasers. Furthermore, the large wavelength-flexibility implies that programmable lithography is possible if one uses masks of heterogeneous rather than identical resonators. In such a scheme, the same mask could be used to define very different patterns using wavelength or polarization tuning. Alternatively, programmable lithography can be based on collective resonances of antenna arrays in which identical resonators are sufficiently closely spaced to be strongly coupled [16, 35]. In such coupled systems different patterns can be written via control over incidence angle, wavelength and polarization [16], or spatio-temporal phasefront shaping [17, 18].

Acknowledgment

We thank Andrej Kwadrin, Ivana Sersic, Chris Rétif, Frank van den Berg, Martin Frimmer and Leon Huisman for help with sample preparation, experiment and data processing. We are very grateful to Dries van Oosten and Matteo Burresi for discussions in the initial stages of the project. This work is part of the research program of the "Stichting voor Fundamenteel Onderzoek der Materie (FOM)," which is financially supported by the "Nederlandse Organisatie voor Wetenschappelijk Onderzoek (NWO)." AFK was supported by a VIDI fellowship funded by NWO.

#146475 - $15.00 USD Received 26 Apr 2011; revised 20 May 2011; accepted 20 May 2011; published 26 May 2011